Accepted version. Published online in *Small* 26 February 2018 DOI 10.1002/smll.201703403

For online published version see: http://onlinelibrary.wiley.com/doi/10.1002/smll.201703403/full

Zinc Oxide nanoparticles and voltage-gated human K_v11.1 potassium channels interact though a novel mechanism.

Stefania Piscopo[1] & Euan R Brown[2*]

1. Stazione Zoologica Anton Dohrn, Villa Comunale, 80121, Naples Italy.
2. Institute of Biological Chemistry, Biophysics and Bioengineering, William Perkin Building, School of Engineering and Physical Sciences, Heriot Watt University, Edinburgh EH14 4AS, UK.

*Communicating author Euan.R.Brown@hw.ac.uk .

2. Institute of Biological Chemistry, Biophysics and Bioengineering,

William Perkin Building,

School of Engineering and Physical Sciences,

Heriot Watt University,

Edinburgh EH14 4AS, UK.

Office (44) (0)131 451 4712 (internal x 4712)

Lab (44) (0) 131 451 4191 (internal x 4191)

Mobile (44) (0)7596 766696

Office WP 2.39

Lab: WP 3.19

Key words: hERG potassium channel, channel gating, Zinc Oxide, nanoparticles, lipid-bilayer.

For online published version see: http://onlinelibrary.wiley.com/doi/10.1002/smll.201703403/full

Accepted version. Published online in *Small* 26 February 2018 DOI 10.1002/smll.201703403

Abstract

Membrane-nanoparticle interactions are important in determining the effects of manufactured nanomaterials on cell physiology and pathology. Here Silica, titanium, zinc, and magnesium oxide nanoparticles were screened against human hERG (K_v11.1) voltage gated potassium channels under whole- cell voltage clamp. 10 µg/ml ZnO uniquely increased the amplitude of the steady state current, decreased the rate of hERG current inactivation during steady state depolarization, accelerated channel deactivation during resurgent tail currents, and showed no significant alteration of current activation rate or voltage dependence. In contrast, $ZnCl_2$ caused increased current suppression with increasing concentration and failed to replicate the nanoparticle effect on decreasing inactivation. The results show a novel class of nanoparticle-biomembrane interaction involving channel gating rather than channel block, and have implications for the use of nanoparticles in biomedicine, drug delivery applications and nanotoxicology.

Introduction

As engineered nanoparticles are increasingly used in multiple applications in manufacturing, and biomedicine, their unique surface to volume ratios, chemical composition and diversity means that their potential interactions with biological processes needs to be continually assessed[1]. With the downstream effects of nanoparticle exposure on cell toxicity becoming clearer [2], the first site of contact of nanoparticles with cells through attachment to, modification of, or penetration through, lipid bilayers and interaction with their constituent intramembrane proteins has received increasing attention. Cationic nanoparticles are capable of inducing nanometer sized holes in supported (artificial)[3] and naturally occurring lipid bilayers [4]. In addition, cationic and anionic nanoparticles are able to induce local membrane fluidity and gelation in lipid bilayers respectively when they bind to the bi-layer surface [5]. As a result of hole formation, NPs may also pass through the membrane in a manner that is independent of endo- or pinocytotic pathways[6].

Cellular lipid bilayers also contain membrane proteins, and nanoparticles also interact with these components in species dependent ways. Small gold nanoparticles directly block ion -channels[7], and cell excitability is altered by the presence of ZnO[8] and nano-Ag[9] in the bathing solution. Other particles, while cytotoxic, do not interfere with channel function[10]. Interpretation of nanoparticle effects are also complicated by nanoparticle behavior in biological solutions, where action could be due to their intrinsic chemistry, genuine 'Nano' effects, or changes due to sedimentation and diffusion of the particles[1,11].

To try to address these issues directly, we characterized and screened a series of engineered nanoparticles (SiO_2, ZnO, MgO, TiO_2) against a model human ion channel (hERG potassium channel) to determine if there were any nanoparticle effects on membrane lipids or channel activity using the whole cell voltage clamp technique and rapid solution exchange (Figure 1). The Voltage Clamp method has the advantage of continuously monitoring membrane integrity, membrane capacitance and is capable of detecting both membrane breakdown and alterations in membrane area in an unambiguous way.

Electrophysiological measurement of heterologously expressed hERG channel activity represents a standard drug screening assay which is widely used to detect potentially harmful 'off-target' drug effects [12], and has been previously used in the nanotoxicology context to demonstrate channel block by ultrafine gold nanoparticles [7] and a lack of effect of cytotoxic CdSe and

CdSe/ZnS particles [10]. As hERG channels have a critical function in shaping the cardiac action potential [13] , and there is a great deal of knowledge about hERG channel biophysics, structure[14], molecular biology and clinical impact [15], the channel presents itself as a good candidate to use to study nanoparticle -ion channel interactions. Using this approach we measured membrane parameters, leak and potassium channel function on addition of a panel of nanoparticles. The results show that of all the types of particle examined, ZnO particles uniquely interact with the hERG channel gating process with implications for cell signaling.

Methods

Nanoparticle Characterization

The hydrodynamic radius (Z-average) of NPs were determined at 20°C using a Zetasizer Nano ZS ZEN3600 (Malvern Instruments Ltd. Malvern, UK) operating with a He-Ne laser at a wavelength of 633 nm and measuring back-scattered light at 173° relative to the incident beam.

NPs were prepared by mixing 2μl of the standard solution (1 mg/ml , 0.1% W/V) which had been sonicated for 20 minutes, with 1 ml of distilled water or filtered solutions (hERG), vortexed for 1 minute and transferred to a disposable folded capillary cell. The samples were run three times with one-minute intervals between measurements for each time point. Changes in particle diameter over time was followed every five minutes for 1 hr to determine the likely behaviour of the particles when added to the experimental chamber. Diameters are given in **Table 1** for one and twenty minute time points for each NP.

As it has been reported that nanoparticle preparations can have significant endotoxin contamination [16], we screened the nanoparticle suspensions in hERG solution at 10 μg/ml of NPS for endotoxin contamination using the LAL chromogenic assay according to the manufacturers' instructions (GenScript, Piscataway, USA).

Electron Microscopy

To further characterize the Nanoparticles in contact with cells, we carried out Scanning Electron Microscopy on fixed material. Briefly, cells were plated onto coverslips and exposed to 10 μg/ml of nanoparticles (Control, SiO_2, ZnO (MB), TiO_2) for twenty minutes . Cells and NPS were then fixed in 2.5 % glutaraldehyde in 0.1 M phosphate buffer at 20 °C (pH 7.3) for 20 minutes, washed in 0.1 M phosphate buffer before immersion in 1% OsO_4, for 20 minutes. Coverslips were dehydrated through 30% to 100% ethanol, critical point dried and sputter coated with 1-2 nm gold-palladium. Coverslips were visualised on a JEOL 6700F scanning electron microscope (JEOL USA, Inc. Peabody USA). Individual particle sizes were estimated by measuring the dimensions of single nanoparticles visible on cells, and on cell processes.

Cell culture

Ready-to-use 'instant' cells were supplied in batch by (Cytocentrics, Db) and stored under liquid nitrogen. The HEK239 cells expressed the voltage sensitive hERG K^+ channel (Kv 11.1 KCNH2). Cells were defrosted prior to use by resuspending them in hERG solution (see below under electrophysiology for solution composition), spun down at 1,000 RPM to remove fragments, resuspended in fresh hERG solution and plated onto glass cover slips. Cells remained viable at room temperature (20°C) for at least eight hours.

Electrophysiology

Currents were recorded from cells at room temperature (20 °C), using the whole cell voltage clamp technique. During recordings, cells were perfused continuously (1 ml/minute) with 'hERG solution' consisting of 140 mM NaCl, 2.5 mM KCl, 2 mM $MgCl_2$, 2 mM $CaCl_2$, 10 mM HEPES, 10 mM Glucose, 15 mM D (+)-Saccharose (pH 7.4, 320 mOsm/kg). Electrodes were pulled with a Sutter Instruments P97 microelectrode puller using borosilicate glass capillaries (Harvard Apparatus Ltd), and filled with intracellular solution (100 mM K-Gluconate, 20 mM KCl, 1 mM $CaCl_2$, 1 mM $MgCl_2$, 10 mM HEPES, 3 mM Phosphocreatine, 11 mM EGTA-KOH, 9 mM D (+)-Sucrose, 4 mM ATP-Mg (pH 7.2, 295 mOsm/kg). 3-5 MΩ resistance pipettes were brought into contact with the cell surface by micromanipulation, GΩ resistance cell-attached seals were obtained by gentle suction, and whole–cell access achieved by rupturing the patch with direct suction. Using an Axoclamp 2B amplifier and a HS-2A-x0.1LU headstage, the cell was clamped to –70 mV. Each voltage clamp protocol was preceded by a 5 mV voltage clamp step which was used later to calculate membrane capacitance and leakage currents (see voltage clamp protocol in Figure 2). Capacitance (C_m) was calculated according to equation 1, where $Q(t)$ is the total charge under the capacitive transient and ΔV is the amplitude of the voltage pulse applied.

$$C_m = Q(t)/\Delta V \qquad (1)$$

The calculation of C_m was carried out using the membrane test feature of Clampfit 10 (Molecular Devices Corporation, 1311 Orleans Dr, Sunnyvale, CA 94089, USA). Current and voltage outputs from the amplifier were digitized through a Digidata 1322A digital acquisition system and stored on an IBM PC. Amplifier, data acquisition system, and software were all from Molecular Devices Corporation (1311 Orleans Dr, Sunnyvale, CA 94089, USA). Cells with holding currents greater or

equal to 100 pA or that developed leakage during perfusion were rejected. All I/V plot plots and data are presented with no compensation for non-linear leakage currents.

Coating ZnO NPs with serum protein

To examine the effect of the generation of a hard protein corona[17], we incubated 10 µg/ml ZnO(MB) particles suspended in hERG sln. in 1% BSA (bovine serum albumin, Sigma-Aldrich, St Louis, USA) for 20 minutes. The resulting solution was perfused over the preparation. Alternatively, hERG sln. containing 1% BSA was perfused over voltage clamped cells either in the presence or absence of ZnO NPs.

Lipid peroxidation

As it has been reported that 10 µg/ml ZnO nanoparticles induce significant lipid peroxidation[18], we induced massive lipid peroxidation by exposing voltage clamped cells to an estimated 10 mM of hydrogen peroxide (H_2O_2) by adding 10 µl of H_2O_2 to hERG solution just before perfusion over the cells. Previous work has estimated that up to 200 µM H_2O_2 produces a maximal peroxidation response in human lymphocytes over 24 hours[19]. The most rapid effects of peroxidation have been reported after 3 hours exposure, [18] thus in our experiments, which lasted a maximum of 20 minutes, changes could not have been generated by peroxidation.

Statistics

Results were tested for significant differences using Student's t-test. In the case of comparison of controls and test results where controls had been conducted in parallel, an unpaired test was applied, where 'before' and 'after' results were compared a paired test was used. All results are presented as mean and standard errors of the mean.

Results

Nanoparticle characterization

Table 1 gives the identities and properties of the Nanoparticles used in this study . It was noted that while TiO_2 and MgO NPs aggregated in hERG solution (this is shown in **Table 1** as an increase in the main peak size with several additional peaks appearing in the DLS measurements with time at over 50 and 100 nm respectively), the hydrodynamic diameters of the other NPs in all cases were remarkably stable during the time course of the experiment. There was an increase in diameter between the manufacturers primary particle sizes (TEM), and the results obtained by DLS, reflecting the fact that DLS measures hydrodynamic diameter. The perfusion system ensured a continuous flow of control and NP loaded solutions with a complete bath exchange every 30s. This approach, along with time- dependent DLS measurements, partly mitigated uncertainties [11,20] about the effective concentration of nanoparticles (continuous mixing), though did not avoid particle aggregation. We were concerned that some of the NP effects could have been due to particle contamination with other substances. Endotoxin contamination of NPs has been reported to have significant effects on cell physiology [16]. We checked the levels of endotoxin using the LAL chromogenic assay and found that a minimal level of endotoxin was present in the samples (below 0.1EU/ml **Figure S1**). For reference, less than 0.16 EU/ml was shown to be ineffective in generating endotoxin stimulated proliferative responses, [16] so it seems that the levels of endotoxin present in the samples were unlikely to account for any of the observed effects.

Electron microscopy

Scanning electron micrographs were taken of representative fixed HEK 239 cells. The results show (**Figure S2**) that when compared to control material, SiO_2 particles form a homogeneous coating of spherical particles around 10-12 nm in diameter over the entire surface of the cells. In contrast, ZnO particles can be seen to adorn the cell surface in a punctate way, and crystal-like forms can be seen adhering to the cell surface (particularly easy to see on the cell processes-arrows). Finally, TiO_2 particles form clustered aggregates on the cell surface. We measured particle diameter from a series of Scanning Electron Micrographs and found (**Table 1** column 7), that particle size was remarkably consistent and quite close to the manufacturers' measurements.

Resurgent tail current analysis

hERG currents were evoked from the cells after stable voltage clamp was established by standardized pulse protocols (holding potential -70 mV, depolarizing pulses between -30 to plus 30 mV, followed by repolarizing pulses to -50 mV (see **Figure 2A**)).

Key features of this potassium channel behavior are an initial outward 'steady-state' current that on increasing depolarization shows increasing inactivation after activation (**Figure2)**, and a distinctive 'resurgent' tail current on repolarization that has a sigmoidal current-voltage relationship that was well fit by a Boltzmann function (**Figure 2B**, black current- voltage relations). The resurgent tail current amplitude was used in an initial screening for all nanoparticles. Such cells were subject to continuous perfusion of extracellular solutions for 20 minutes. Membrane capacitance, leak current (defined as the difference between I=0 and the holding current), steady state current, and the amplitude of the resurgent tail current were monitored once every minute before, during, and after application of NPs (**Figure 3**).

No significant rundown or alteration of hERG current properties (current amplitudes, activation inactivation of resurgent tail or steady state currents) was observed under control conditions (**Figure 3A & B**). NPs were added to the experimental extracellular solution at dilutions of between 1/1000-100 x and were applied to the system by the perfusion system. NPs were added to the bath perfusion system seven minutes after stability was obtained. Neither SiO_2, TiO_2, nor MgO had significant effects on resting membrane conductance, leak, or the resurgent tail current (**Figure S3A**). **Figure 3B** shows the application of SiO_2 compared to control (null addition). In contrast ZnO (10 μg/ml), increased the amplitude of the resurgent tail current by an average of around 30 % (**Figure 3C**). Even on prolonged washing this increase in tail current amplitude was not reversible (not shown). We applied different concentrations of ZnO NPs to better understand the dose response relationship in the range of 0.1-100 μg/ml (**Figure S3B**). The results show an increasing effect on increasing concentration, but we were unable to fit the data well with a sigmoidal function.

Detailed investigation of the effect of ZnO on tail currents

To better understand the process underlying the resurgent tail current increase on ZnO addition, an analysis of current kinetics was carried out.

i Activation Kinetics

The rising phase of the whole-cell K^+ current for the first 500 ms after depolarization from -70 mV was well fit by a single rising exponential function (formula 2 and see **Figure S4A**):

$$f(t) = \sum_{i=1}^{n} A_i \; e^{-t/\tau_i} + \; C \qquad (2)$$

A time constant of around 35 ms was obtained for the rising phase and the application of ZnO had no discernible effect on current activation. Indeed, the current activation rate was unchanged after 20 minutes (**Figure S4B**).

ii Steady-state current

The steady state current was measured 0.5 s before the repolarization phase (indicated in **Figure 4A**). The addition of ZnO was found to increase the steady- state current by around 100% (**Figure 4B**) though with a high degree of variability from cell to cell.

Control values for the steady state current were stable for the duration of the experiment. This increase in current was clearly due to a decline in the strong inactivation evident in the steady state current after the first 500 ms of activation. A further analysis was carried out to estimate how the inactivation rate decreased by fitting a straight line to the steady-state current after the current peaked (**Figure S5A**). The negative slope of the current fit was transformed into a positive slope by the addition of ZnO, while the inactivation rate in controls was remarkably stable over time (**Figure S5B**). This suggested that the increase in the resurgent tail current was the result of an increase in the steady-state current driven by a decrease in the prominent inactivation on depolarization.

iii Resurgent tail current deactivation

As the result of kinetic analysis suggested that the effect was not due to a change in activation kinetics but rather a decrease in inactivation, we examined the deactivation rate of the resurgent tail currents. The tail currents were well fit with a double exponential function consisting of fast and slow components. In control material there was a gradual slowing of the deactivation rate

which was reflected by an increase in the time constant of both fast and slow components with time. In contrast to this trend, both slow and fast deactivation rates became faster on application of ZnO (**Figure 5**). Both fast and slow deactivation rates increased by around 60%.

iv Current-voltage relations

As the screening involved repeatedly testing the membrane current by stepping the membrane voltage to 20 mV from -70 mV over a 20 minute period, a potential explanation for the 'increase' in membrane current on ZnO addition could have been a substantial shift in the current voltage relations of the tail and steady-state currents. To examine this possibility, the current-voltage relations of the hERG resurgent tail currents were plotted for voltage steps between -30- +30 mV in the presence and absence of ZnO (**Figure S6**). There was no shift in normalized current voltage relations for the tail currents. Instead, the amplitude of the currents increased in parallel across the full voltage range. This confirms that the increase in current cannot be explained by a shift in current voltage relations.

Changes in the lipid environment around the hERG channel

As it has been established in artificial lipid bilayers that addition of membrane penetrating/ membrane incorporated NPs could be detected by measuring membrane capacitance (C_m) [21], we continuously monitored C_m by applying a brief 5 mV depolarizing step as an integral part of every voltage clamp protocol prior to any voltage steps designed to evoke voltage activated currents (see e.g. Figure 2). This had the additional advantage of allowing continuous monitoring of membrane leak currents. The results show (**Figure S7**) that the cells had a mean capacitance of around 22 pF and that application of ZnO (or indeed any other NP type) did not significantly alter C_m.

Comparison with free Zinc ions

It is well known that hERG ion channels are blocked by Zn^{2+}[22]. We applied a range of $ZnCl_2$ concentrations to voltage-clamped cells to establish if the ZnO effects could be explained by the local release of significant quantities of Zn^{2+} from the NPs. The results show the $ZnCl_2$ sensitivity of the hERG current where effects can be detected between 0.01-20 mM Zn^{2+}. Zn^{2+} has a blocking effect with an EC_{50} of around 800 μM $ZnCl_2$ (**Figure 6 A&B**).

Significantly, no increase in steady state current or tail current was noted after addition of $ZnCl_2$ pointing to the mechanism of action of ZnO as being through a nanoparticle-channel interaction rather than a dissolved free- ion channel- block. To further examine this relationship we plotted all the kinetic parameters obtained in lower concentrations of $ZnCl_2$ against the mean and SEM obtained in 10 µg/ml ZnO (**Figure S8 A-F**). No significant effects of $ZnCl_2$ were seen on kinetics that were similar to these seen on ZnO addition. The only significant alterations noted were a small increase in activation kinetics in 200 µM $ZnCl_2$.

Coating ZnO NPs and exposing membranes to serum protein

We hypothesized that the effect seen on addition of ZnO was a possible NP-ion channel interaction. To begin to investigate this we examined the effect of coating ZnO NPs with protein before adding them to the experimental chamber. It has been established that exposure of ZnO nanoparticles to serum proteins results in the formation of a 'hard' protein corona around the particle[17]. 10 µg/ml ZnO nanoparticles were incubated with 1% bovine serum abumin (BSA) for 20 minutes and the solution added to the experimental chamber. Recordings over 20 minutes revealed no alteration in current or membrane properties (**Figure S3A**). Similarly, after addition of ZnO nanoparticles and induction of the ZnO effect, 1% serum albumin was added to the bath and resulted in no reversal of the ZnO effect (Figure S3A). This was similar to the lack of reversal of the ZnO effect seen on repeated washing (not shown). BSA addition alone had no effect on hERG currents (Figure S3A).

Influence of lipid peroxidation

It has been reported that exposure to 10 µg/ml ZnO results is in significant lipid peroxidation,[18]. Although peroxidation takes around 3 hours to manifest itself, and here experiments lasted a maximum of 20 minutes, we decided to test the idea that the changes we observed could be due to the early effects of lipid peroxidation or alteration of protein components in the cell membrane. We exposed the cells to 0.1% H_2O_2 in extracellular medium for 20 minutes while continuously monitoring membrane integrity. We saw no changes (increases of decreases or indeed any other alterations) in ion channel or membrane properties **(Figure S9)**.

Conclusions

Nanoparticles

Our results reveal a novel mode of nanoparticle-biomembrane interaction through likely modification of channel gating mechanisms by ZnO either by direct interaction with the channel or *via* alterations in the properties of the surrounding lipid bilayer. The data extend our knowledge of nanoparticle action by showing that SiO_2, TiO_2, and MgO do not interact directly to disrupt the lipid bilayer or the model K^+ channel (hERG) used in these studies.

Nanoparticle characterization

Analysis using DLS showed the difficulties in comparing the effects of different NPs on cell physiology. While SiO_2 remained suspended in the test solution, ZnO began to aggregate slowly around 20 minutes. In comparison, TiO_2 and MgO NPs rapidly aggregated. Although the former particles had no demonstrable effect on the ion channel, any action may have been masked as the rapid particle aggregation presumably led to a lower concentration of free particles available around the primary particle size. The problems of establishing what cells and tissue are actually exposed to during NP application have been outlined before and are exacerbated the longer the material is in contact with NPs [20]. Equally, sedimentation and aggregation significantly alter dose-response relationships of NPs in culture conditions, [11] and presumably contributed to the non-standard dose response relationship we found between ZnO and hERG. It is well known that the continuous transformation of NPs in biological solutions may alter the outcome of toxicological experiments. For example, although TiO_2 NPs are regarded as non-toxic, they were shown to negatively impact zebrafish development[23] . When the toxicity of TiO_2 NPs was compared to their dissolved salt equivalents however, there was no increased nano-toxicity effect, [24]. These apparently conflicting results often occur when 'long' exposures to NPs are studied.

Nanoparticle effects on lipid bilayers

Bearing in mind the issues outlined above, combining DLS analysis with the hERG screen allowed us to test rapidly a range of nanoparticles on biological membranes and ion channels with a reasonable certainty of their state within the experimental time period. In standard toxicology experiments in cultured cell conditions, typical exposure times range from two hours to several days with NP concentrations ranging from 10- 100 μg/ml[25]. Our approach had the advantage of

determining the interactions in a matter of minutes and we deliberately tested particles at the lower end of the range used in toxicology experiments (from 0.1 to 100 μg/ml). Our first concern was to determine the extent of interaction of NPs with the lipid bilayer of the cells. Under voltage clamp conditions, when a holding potential is set (in this case -70 mV), the amount of current that has to be continuously injected into the clamp circuit to maintain this potential (termed holding or leakage current) is a direct indication of the membrane resistance according to Ohms law. An increased permeability of the membrane bilayer would be reflected by an increase in this current through the clamp circuit. This kind of leakage current associated with nanoparticle- induced nanoscale 'holes' has been previous reported using the voltage clamp technique[2,4]. This value was always used as an initial (and continuous) quality control of the membrane state. Initial leakage currents after access to the whole cell- mode of recording[26] of greater that -100 pA were rejected at the outset and the current was continuously monitored during the experiment. We did not observe any changes in membrane holding-current during these experiments as a result of the addition of NPs. If anything, the quality of the seals tended to gradually improve over the course of the experiment and this led to some moderate changes (improvements) in clamp quality. This lack of change in holding current does not mean that nanoparticles do not interact with the surface of the lipid bilayer. Indeed, in the case of SiO_2, a distinct size -dependent Van der Waals interaction with artificial lipid monolayers has been reported, [27] and some formulations of ZnO also interact with lipid monolayers in the same way (although the formulation we used here of metals basis ZnO did not, [28]). The same membrane stability was observed for MgO and TiO_2 NPs. The close contact of NPs with the lipid bilayer was reinforced by our results of scanning electron microscopy which shows many particles on or close to the cell surface. An additional issue is that it is known that changes in the local lipid environment have been shown to alter hERG channel gating [29] by translocation of channels into lipid raft- like structures [30]. Taken with recent work on cationic nanoparticles, which show that they induce a local gel phase in otherwise liquid lipid bilayers[5], we considered whether local lipid changes could contribute to the ZnO effect. We attempted to ascertain if the lipid environment was altered by ZnO NPs by measuring cell capacitance. We found no evidence of changes in cell capacitance after NP addition, however several considerations indicate that the method we used may not be sensitive enough to definitively rule out local lipid changes. Previously it has been shown in artificial lipid bilayers that NP interactions with lipid can be detected as an increase in membrane capacitance (C_m). In these experiments, using artificial black lipid bilayers of around 150 pF, addition of 1 mg/ml NP increased capacitance by around 5 %,

[21]. In our cells with a capacitance of 20 pF, and NP concentrations of 10 µg/ml, we would need to be able to resolve changes of less than 1 pF and our variance was around 4-5 pF. Clearly on this basis, we cannot rule out changes in lipid composition.

Nanoparticle effects on hERG channels

Having determined that membrane resistance remained stable in the range of NPs used in these experiments, we set up a simple screening protocol whereby the hERG channel current was evoked by depolarizing voltage steps to 20 mV from the holding potential of -80 mV and resurgent tail currents were generated by repolarization to –50 mV. These currents were evoked once a minute for 20 minutes. Nanoparticles were perfused over the cells after 7 minutes of control recording. Controls were also run for 20 minutes for comparison without the addition of NPs . The results show that under control conditions there were no significant changes in current amplitudes and currents were maintained for a least 20 minutes without any significant 'rundown'. No changes in current amplitude were noted on addition of SiO_2, TiO_2, or MgO. In contrast ZnO addition evoked significant and irreversible changes in hERG current behaviour. The results from the screening showed a significant increase in current amplitude (steady state) and resurgent tail current peak.

To examine this effect of ZnO in more detail, a kinetic analysis of hERG currents was carried out. In a separate series of experiments a wider range of depolarizing steps (between -30 and +30 mV were imposed and the results show that there was no underlying shift in voltage dependence of the tail current (which could have explained the increase). Analysis of activation, inactivation and deactivation shows that while activation is unaffected, deactivation is more rapid than under control conditions. The steady- state current shows a lesser degree of inactivation during depolarization and this results in less rectification.

To explain these changes we need to examine hERG gating. hERG channels have unusual gating kinetics where activation and inactivation have distinctly different rate constants, characterized by slow activation, fast inactivation and strong rectification [31]. This gives the hERG channel its characteristic properties so crucial in its role in controlling cardiac action potential repolarization and interbeat stability [13]. Inactivation in K^+ channels can be N-type [32] or C- type [33] or a combination of both (where 'N' and 'C 'refer to the process of inactivation predominantly occurring in the regions of the N and C terminals of the channel protein). In hERG channels it

appears that N-type inactivation is absent or minimal, and C- type dominates [34]. This means that the inactivation mechanism is located in the C- terminal region of the protein. The structural determinants of inactivation are not located a single part of the protein but are complex interactions between a series of moieties. A recent summary (based on mutagenesis scanning and rate equilibrium free energy relationship (REFER) analysis), indicates that this complex process may involve at last nine interconnected steps, sequencing through, the loss of an external K^+, from the pore helix, the S5 helix, the S5P linker, the S4 helix, the S4-S5 linker, the S6 helix, the pore helix and the rearrangement of the channel selectivity filter[35]. As our results indicate that ZnO NPs are not penetrating the lipid bilayer it seems likely that they interact with the external face of the channel either directly or *via* alterations in the local lipid environment. Of the entities described above in the inactivation sequence, only the S5P linker between the S5 and core helix (P), and the pore helix face the external surface of the lipid bilayer, and are available to interact with the NPs.

The view that the S5P linker could be involved is supported by experiments where M-eag and hERG channel chimeras were made. M-eag K^+ channels normally show no inactivation and little rectification though they are thought to be closely related to hERG channels. Transfer of portions of the hERG P region (core helix) and half of S6 (including the S4-S5 linker) confer hERG like inactivation and rectification on M-eag. While transfer of similar portions of M-eag to hERG remove most of the hERG channels distinctive inactivation and rectification [36]. As the rectification resides in the selectivity filter it seems likely that ZnO NPs are interacting with the protein here. It would be of great interest in the future to examine the effect of ZnO NPs on closely related channels such as M-eag and on point mutations associated with hERG implicated in arrhythmias [37] which involve changes in the C -terminal region. Alternatively, as movement of hERG channels into lipid-rafts has been shown to suppress currents, [38] it seems also possible that movement out of lipid rafts could enhance currents in the manner seen here.

Likely models of action of ZnO

ZnO is a polar crystalline 'Wurtzite' solid [39] with a tendency to aggregate and release Zn^{2+} in solution [40]. Detailed kinetic studies using an electrochemical method to measure the free Zn^{2+} concentration have shown that when ZnO is placed in solution, after an initial release period, an equilibrium is achieved between the ZnO concentration and Zn^{2+} [41]. At nearly neutral pH, the

ratio between bulk Zn and zinc ions is initially 1:0.01 and rises after 40 minutes to a steady ratio of 1:0.1 [41]. The formula weight of the ZnO powder was 81.37 which means Zn was thus added to the cells at a concentration of 0.123 mM (10 µg/ml). Assuming the same solubility ratios as David et al [41], this would set the lower and higher limits of Zn^{2+} in solution as at 1 -12 µM. It can be clearly seen in the scheme in **Figure S7** that this range of Zn^{2+} has apparently no effect on channel currents. At Zn^{2+} concentrations of 0.5 mM and above, channel block is evident (**Figure 6**), as previously described [22]. It therefore also seems unlikely that hERG channels are modulated by serum Zn^{2+} in this range.

Serum Zn^{2+} in adult humans is around 10-17 µM [42] and as around 80 % of Zn is bound to plasma proteins such as albumin, under physiological conditions, free zinc could be present at no more than 1-2 µM [43]. The possibility remains however that the presence of *both* free Zn^{2+} and NPs in very close proximity to the channel are necessary for the changes we observed in ion channel currents. We were able to partially test this idea with the results of the experiments where we added BSA after the channel effect had been observed. We were unable to detect any reduction in current under these circumstances. In this situation BSA would have the dual effect of binding to available free NPs and absorbing free Zn^{2+}. In experiments where ZnO NPs were mixed with BSA prior to addition to the experimental chamber, the NP effect was neutralized completely. These considerations effectively rule out the possibility that the effect seen on hERG K^+ currents can be attributed to a significant accumulation of Zn^{2+} at the surface of the particle or in the bulk solution and point to a likely nano-membrane protein/lipid interaction.

Thus the likely mode of action on channel gating is either through a direct interaction with the ZnO nanoparticle or through an interaction with the lipid environment of the hERG channel. Two opposing forces determine the stability and fixed charge of NPs in solution; electrostatic repulsion vs. Van der Waals forces [44] (described by DLVO theory: Derjaguin, Landau, Verwey and Overbeek). As ZnO has an isoelectric point between 9-10 the NPs will have a strong positive charge at physiological pH [45], however this charge will be screened in bulk solutions by counter ions (this is seen in Table 1 where the Zeta potential becomes nearly neutral in hERG solution). NPs will be able to exert an effect only at interfaces especially if negatively charged elements are encountered which can replace the bulk counter ions, and where Van der Walls forces rather than opposing, will combine in relatively strong interactions. Such interactions with gating in biological membranes have been shown to be theoretically feasible [46]. Again if we consider the outwardly facing S5P loop of the hERG channel that

is so critical in inactivation in hERG (see above), it has been found that substitution of negatively charged Aspartate (D) at position 591 with positively charged Arginine (R) enables reduced inactivation of the current in much the same way as we see here [47]. It seems possible that a closely opposed positively charged NP could neutralise (and perhaps weakly bind to), the negatively charged residue. It would be of great interest to see if modifications of the surface charge on ZnO and/or mutations of position 591 could alter this result.

Irreversibility and dose dependence

We would like to underline the finding that we were unable to reverse the ZnO effect even after 20-40 minutes of continuous washing with fresh hERG solution. This suggests that the interaction with NP is irreversible and points to either a transformation in the lipid bilayer or binding to the channel. We also tried to establish the dose response relationship between ZnO and the increase in the hERG current. The data was not well fit with a dose response curve though it was clear that the effect increased with increasing concentration. This experiment was problematic because of the lack of wash-off and as many of the seals became unstable at >100 µg/ml.

Cardiac risk

Considering the importance of hERG in controlling cardiac beat stability, this finding has implications for the choice of NPs to be used in biomedicine which is a rapidly a growing field [48]. In the first instance alterations in hERG channel conductance in the range shown here by modest concentrations of ZnO NPs could alter the cardiac action potential and subsequent contractility by decreasing the intracellular Ca^{2+} transient. Thus ZnO may be considered to represent a cardiac risk factor if used in formulations (though increasing the hERG current effectively increases beat stability). ZnO is normally considered to be relatively harmless and is used regularly in e.g fluorescence, magnetic resonance, and positron emission tomography imaging as well as in topical and systemic application [48]. In our experiments, ZnO altered channel gating when protein free media was used, the protein 'corona' which rapidly forms around NPs (including ZnO) when serum containing media is used [17,49], negated this effect. It seems likely that the protein coating would screen any charge effects or binding seen in our experiments. We were unable to reverse the effects seen on hERG with long-term washing (up to two hours) and thus is seems possible that there is an irreversible interaction with the channel protein or the lipid bilayer. Further experimentation with higher resolution C_m measurements will be required to establish which of the two mechanisms are most likely and thus reach a conclusion on the potential risk to cardiac

health including experiments with cardiomyocytes. Finally it is worth noting there are few drugs designed to work on the hERG current that act to increase the current density on depolarization. The vast majority of compounds known to interact on hERG do so to block or inhibit channel activity and are thus not particularly useful in rectifying hERG current deficiencies that lead to arrhythmias [13,50].

Conclusions

Through screening a panel of nanoparticles against bio-membranes and a model K^+ ion channel, we show that most NPs do not interact with either membrane or channel. However, ZnO nanoparticles exhibit a strong effect on channel gating such that the hERG channel loses some of its normally strong rectification. The results suggest that this is mediated though a novel ion channel -NP interaction.

References

[1] A. E. Nel, L. Mädler, D. Velegol, T. Xia, E. M. V. Hoek, P. Somasundaran, F. Klaessig, V. Castranova, M. Thompson, *Nat. Mater.* **2009**, *8*, 543.

[2] H. Johnston, D. M. Brown, N. Kanase, M. Euston, B. K. Gaiser, C. T. Robb, E. Dyrynda, A. G. Rossi, E. R. Brown, V. Stone, *Toxicol. In Vitro* **2015**, *29*, 1172.

[3] A. Mecke, S. Uppuluri, T. M. Sassanella, D. K. Lee, A. Ramamoorthy, J. R. Baker, B. G. Orr, M. M. Banaszak Holl, in *Chem. Phys. Lipids*, **2004**, pp. 3–14.

[4] J. Chen, J. A. Hessler, K. Putchakayala, B. K. Panama, D. P. Khan, S. Hong, D. G. Mullen, S. C. Dimaggio, A. Som, G. N. Tew, A. N. Lopatin, J. R. Baker, M. M. B. Holl, B. G. Orr, B. G. Orr, *J. Phys. Chem. B* **2009**, *113*, 11179.

[5] B. Wang, L. Zhang, S. C. Bae, S. Granick, *Proc. Natl. Acad. Sci.* **2008**, *105*, 18171.

[6] Y. Roiter, M. Ornatska, A. R. Rammohan, J. Balakrishnan, D. R. Heine, S. Minko, *Nano Lett.* **2008**, *8*, 941.

[7] A. Leifert, Y. Pan, A. Kinkeldey, F. Schiefer, J. Setzler, O. Scheel, H. Lichtenbeld, G. Schmid, W. Wenzel, W. Jahnen-Dechent, U. Simon, *Proc. Natl. Acad. Sci. U. S. A.* **2013**, *110*, 8004.

[8] J. Zhao, L. Xu, T. Zhang, G. Ren, Z. Yang, *Neurotoxicology* **2009**, *30*, 220.

[9] Z. Liu, G. Ren, T. Zhang, Z. Yang, *Toxicology* **2009**, *264*, 179.

[10] C. Kirchner, T. Liedl, S. Kudera, T. Pellegrino, A. Muñ Oz Javier, H. E. Gaub, S. Sto, N. Fertig, W. J. Parak, **n.d.**, DOI 10.1021/nl047996m.

[11] E. C. Cho, Q. Zhang, Y. Xia, *Nat. Nanotechnol.* **2011**, *6*, 385.

[12] J. Dunlop, M. Bowlby, R. Peri, D. Vasilyev, R. Arias, *Nat. Rev. Drug Discov.* **2008**, *7*, 358.

[13] M. C. Sanguinetti, C. Jiang, M. E. Curran, M. T. Keating, *Cell* **1995**, *81*, 299.

[14] W. Wang, R. MacKinnon, *Cell* **2017**, *169*, 422.

[15] J. I. Vandenberg, M. D. Perry, M. J. Perrin, S. A. Mann, Y. Ke, A. P. Hill, K. Channels, *Physiol Rev* **2012**, *92*, 1393.

[16] H. Vallhov, J. Qin, S. M. Johansson, N. Ahlborg, M. A. Muhammed, A. Scheynius, S. Gabrielsson, *Nano Lett.* **2006**, 1682.

[17] Z. J. Deng, G. Mortimer, T. Schiller, A. Musumeci, D. Martin, R. F. Minchin, *Nanotechnology* **2009**, *20*, 455101.

[18] V. Sharma, R. K. Shukla, N. Saxena, D. Parmar, M. Das, A. Dhawan, *Toxicol. Lett.* **2009**, *185*, 211.

[19] Y. H. Siddique, G. Ara, M. Afzal, *Dose-Response* **2012**, *10*, 1.

[20] D. Walczyk, F. B. Bombelli, M. P. Monopoli, I. Lynch, K. A. Dawson, *J. Am. Chem. Soc.* **2010**, *132*, 5761.

[21] R. P. Carney, Y. Astier, T. M. Carney, K. Voitchovsky, P. H. Jacob Silva, F. Stellacci, *ACS Nano* **2013**, *7*, 932.

[22] J. M. Anumonwo, J. Horta, M. Delmar, S. M. Taffet, J. Jalife, *Biophys. J.* **1999**, *77*, 282.

[23] J. Wang, X. Zhu, X. Zhang, Z. Zhao, H. Liu, R. George, J. Wilson-Rawls, Y. Chang, Y. Chen, *Chemosphere* **2011**, *83*, 461.

[24] L. C. Wehmas, C. Anders, J. Chess, A. Punnoose, C. B. Pereira, J. A. Greenwood, R. L. Tanguay, *Toxicol. reports* **2015**, *2*, 702.

[25] H. Jeng, J. Swanson, *J. Environ. Sci. Heal. Part A* **2006**, *41*, 2699.

[26] B. Sakmann, E. Neher, *Single-Channel Recording*, Springer, **2009**.

[27] A. Vakurov, R. Brydson, A. Nelson, *Langmuir* **2012**, *28*, 1246.

[28] A. Vakurov, G. Mokry, R. Drummond-Brydson, R. Wallace, C. Svendsen, A. Nelson, *J. Colloid Interface Sci.* **2013**, *404*, 161.

[29] Y. Bai, J. Wang, H. Shan, Y. Lu, Y. Zhang, X. Luo, B. Yang, Z. Wang, *Cell. Physiol. Biochem.* **2007**, *20*, 429.

[30] S. B. Ganapathi, T. E. Fox, M. Kester, K. S. Elmslie, *Am. J. Physiol. Cell Physiol.* **2010**, *299*, C74.

[31] D. R. Piper, M. C. Sanguinetti, M. Tristani-Firouzi, *Novartis Found. Symp.* **2005**, *266*, 46.

[32] T. Hoshi, W. N. Zagotta, R. W. Aldrich, *Science* **1990**, *250*, 533.

[33] K. L. Choi, R. W. Aldrich, G. Yellen, *Proc. Natl. Acad. Sci. U. S. A.* **1991**, *88*, 5092.

[34] P. L. Smith, T. Baukrowitz, G. Yellen, *Nature* **1996**, *379*, 833.

[35] M. D. Perry, C.-A. Ng, S. A. Mann, A. Sadrieh, M. Imtiaz, A. P. Hill, J. I. Vandenberg, *J. Physiol.* **2015**, *593*, 2575.

[36] I. M. Herzberg, M. C. Trudeau, G. A. Robertson, *J. Physiol.* **1998**, 3.

[37] M. C. Sanguinetti, M. Tristani-Firouzi, *Nature* **2006**, *440*, 463.

[38] S. B. Ganapathi, T. E. Fox, M. Kester, K. S. Elmslie, *Am. J. Physiol. Cell Physiol.* **2010**, *299*, C74.

[39] H. Schulz, K. H. Thiemann, *Solid State Commun.* **1979**, *32*, 783.

[40] Q. Mu, C. A. David, J. Galceran, C. Rey-Castro, Ł. Krzemiński, R. Wallace, F. Bamiduro, S. J. Milne, N. S. Hondow, R. Brydson, G. Vizcay-Barrena, M. N. Routledge, L. J. C. Jeuken, A. P. Brown, *Chem. Res. Toxicol.* **2014**, *27*, 558.

[41] C. A. David, J. Galceran, C. Rey-Castro, J. Puy, E. Companys, J. Salvador, J. Monné, R. Wallace, A. Vakourov, *J. Phys. Chem. C* **2012**, *116*, 11758.

[42] M. Rükgauer, J. Klein, J. D. Kruse-Jarres, *J. Trace Elem. Med. Biol.* **1997**, *11*, 92.

[43] J. Lu, A. J. Stewart, P. J. Sadler, T. J. T. Pinheiro, C. A. Blindauer, *Biochem. Soc. Trans.* **2008**, *36*, 1317.

[44] B. Derjaguin, L. Landau, *Prog. Surf. Sci.* **1993**, *43*, 30.

[45] A. Degen, M. Kosec, *J. Am. Ceram. Soc.* **2003**, *86*, 2001.

[46] I. Lundström, *FEBS Lett.* **1977**, *83*, 7.

[47] C. E. Clarke, A. P. Hill, J. Zhao, M. Kondo, R. N. Subbiah, T. J. Campbell, J. I. Vandenberg, *J. Physiol.* **2006**, *573*, 291.

[48] Y. Zhang, T. R. Nayak, H. Hong, W. Cai, *Curr. Mol. Med.* **2013**, *13*, 1633.

[49] M. P. Monopoli, D. Walczyk, A. Campbell, G. Elia, I. Lynch, F. B. Bombelli, K. A. Dawson, *J. Am. Chem. Soc.* **2011**, *133*, 2525.

[50] D. Thomas, C. A. Karle, J. Kiehn, *Curr. Pharm. Des.* **2006**, *12*, 2271.

Acknowledgements

This project and Stefania Piscopo were supported by the EU FP7 ENNSATOX project NMP4-SL-2009-229244. We thank Mr Gabriele Ferrandino for technical support during the project and Mr F Iamunno of the Electron Microscopy service, both of the Stazione Zoologica Anton Dohrn, Naples , Italy.

Competing interests

The authors declare they have neither financial nor non-financial competing interests with respect to this work.

Figures and Figure legends

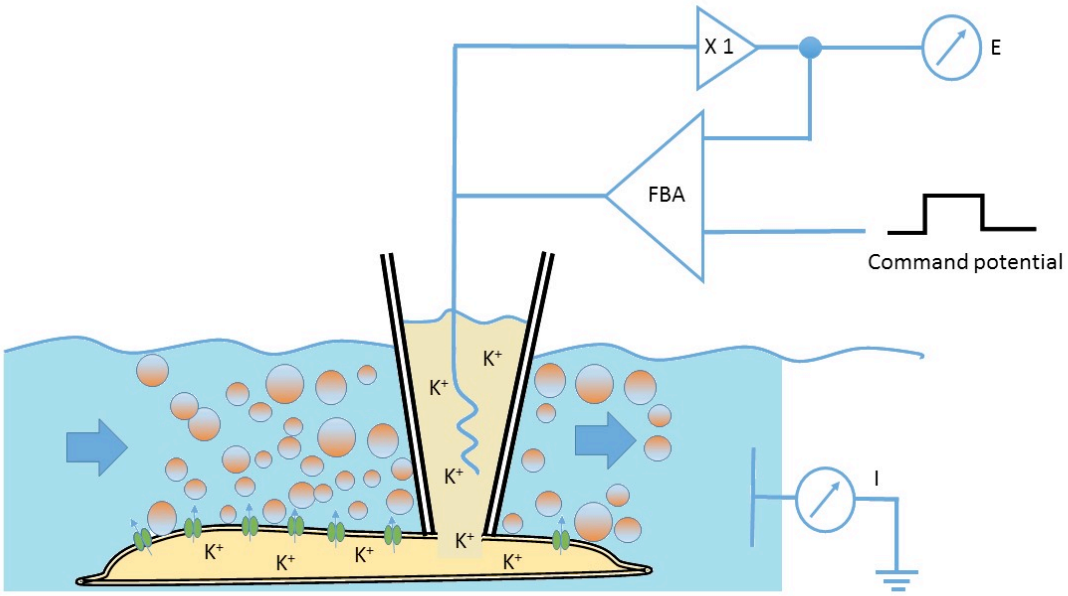

Figure 1. Diagram of the experimental setup. Solutions (including nanoparticles) were perfused over cultured HEK 239 cells expressing hERG potassium channels (green symbols). Cells were voltage clamped through glass micropipettes via a feedback amplifier (FBA). Current (I) was measured as was electrical potential (E). Command potentials were applied to the FBA circuit to evoke membrane currents. The internal environment of the cell was also rapidly dialyzed through the pipette with a K^+ -rich solution.

Figure 2

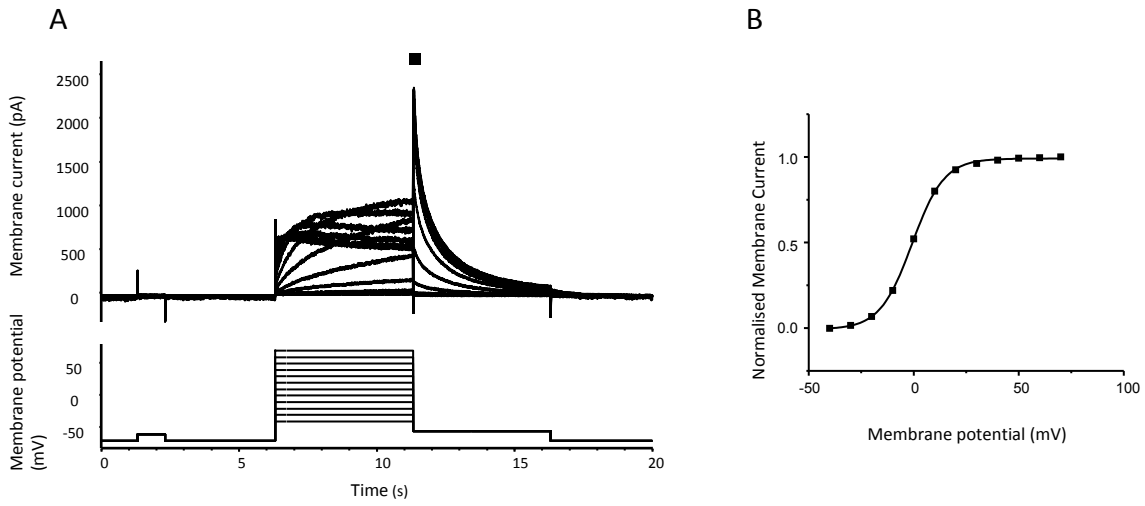

Figure 2. Current/voltage relations of hERG currents in HEK239 cells. A) Voltage clamp protocol. The holding potential was -70 mV. A brief 5 mV depolarizing pulse to check leakage and capacitive currents was followed by 12 x depolarizing 10 mV incremental steps to +80 mV. After 5 seconds depolarization the potential was stepped to -50 mV. The currents evoked show two main characteristics: a slow outward current that inactivates strongly during increasingly positive depolarizations and a prominent resurgent tail-currents on repolarization to -50 mV. B) Current-voltage relations of the currents in A). The outward tail currents measured at their peak (■) show a perfect Boltzmann -like relationship which was well fit by the formula (black curve): normalized tail current= $1/\{1 +\exp((V_{0.5}-)/K)\}$. $V_{0.5}$ was -0.8 mV and K was mV 7.6 (slope factor) in this case (for average values see the legend of Figure S9).

Figure 3

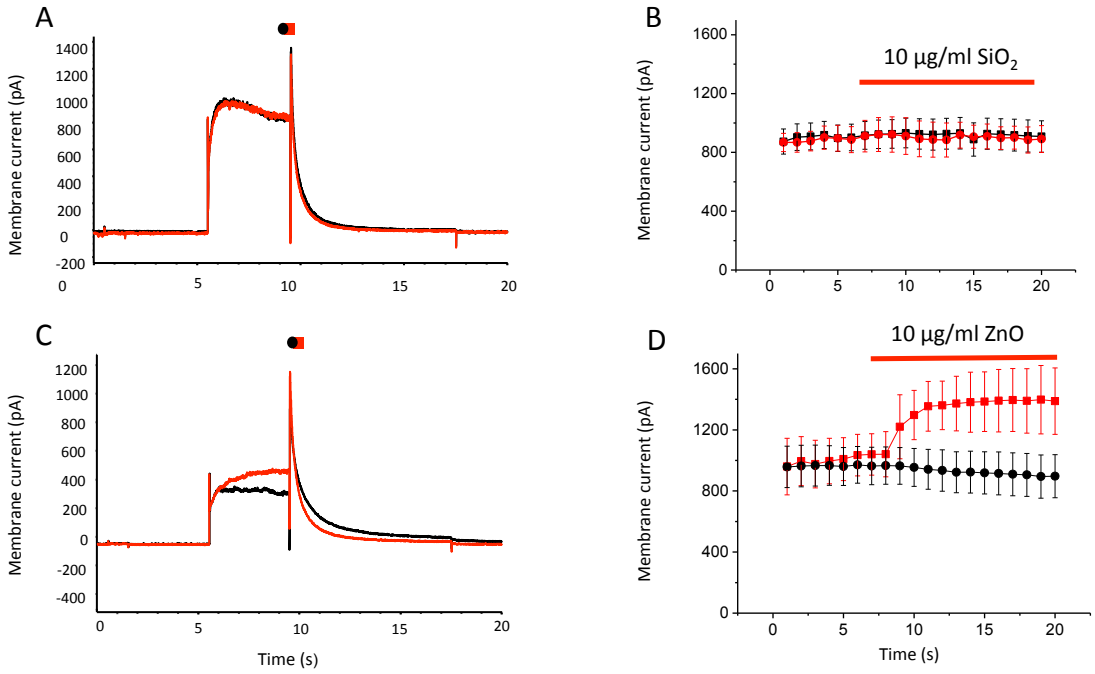

Figure 3. Nanoparticle addition and hERG peak resurgent tail- currents. First and last of twenty currents evoked at one minute intervals from a holding potential of -70 mV, stepped to +20 mV and repolarised to -50 mV before stepping back to -70 mV. A) Addition of 10 µg/ml of SiO_2, B) Peak tail currents evoked by the pulse protocol in A). Tail currents are plotted against experimental time (20 minutes) as the average and standard error of the mean (SEM). Six experiments where SiO_2 was added on the seventh pulse (■ , SiO_2 addition shown by the red bar) are plotted against six control (no addition, ●) to show the stability of the preparation. C) Example of first and last currents under the same conditions as A showing the effect of 10 µg/ml ZnO addition D) Peak tail currents evoked by the pulse protocol in A). Tail currents are plotted against experimental time (20 minutes) as the average and standard error of the mean (SEM). Six experiments where ZnO was added on the seventh pulse (■) are plotted against six controls (no addition ●). Samples from 12-20 minutes are significantly different ($P<0.05$).

Figure 4

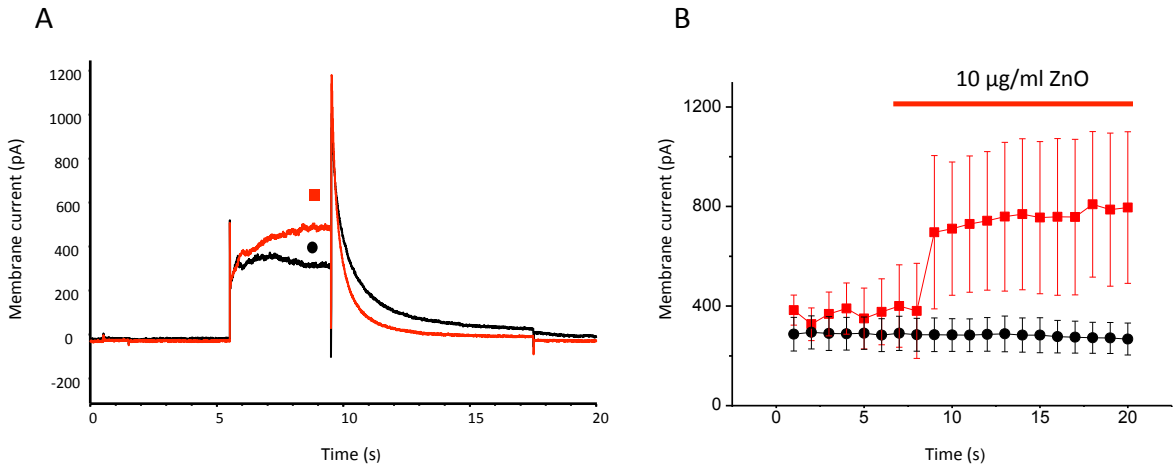

Figure 4. Nanoparticle effects on 'steady state' hERG currents. First and last of twenty hERG currents evoked at one minute intervals from a holding potential of -70 mV, stepped to +20 mV and repolarised to -50 mV before stepping back to -70 mV. A) Addition of 10 µg/ml of ZnO. B) Currents evoked by the pulse protocol in A). Currents are plotted against experimental time (20 minutes) as the average and standard error of the mean (SEM). Six experiments where ZnO was added on the seventh pulse (■, ZnO addition shown by the red bar) are plotted against six control (no addition, ●) to show the stability of the preparation.

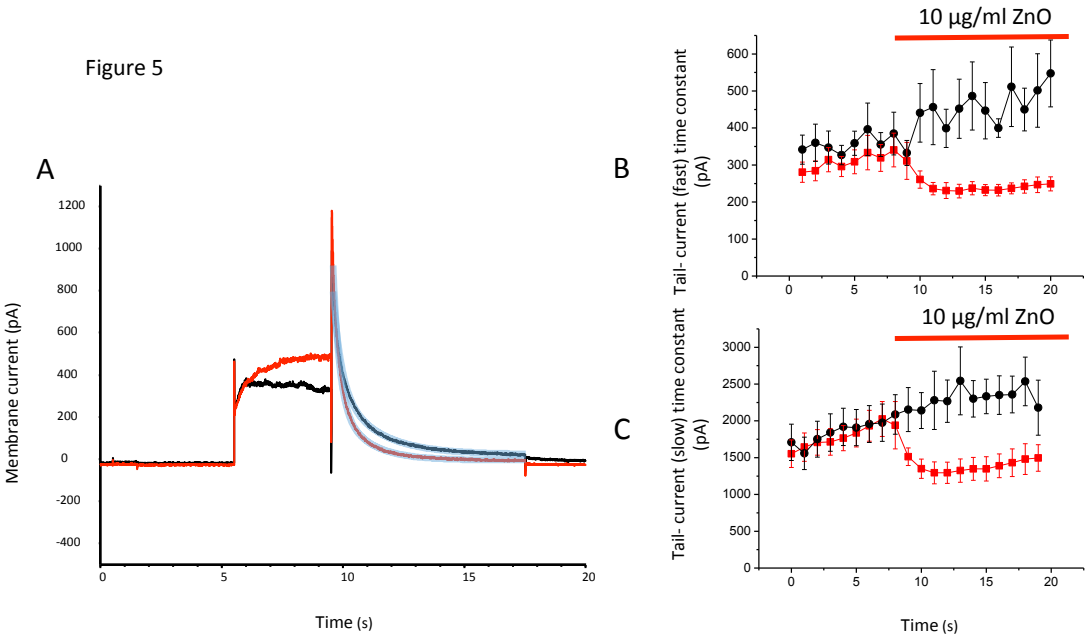

Figure 5. ZnO action on the inactivation rate of the resurgent tail current. A) A double exponential functions were fitted to tails of the resurgent tail- currents. B) and C). The fast and slow inactivation time constants were plotted against experimental time (20 minutes) as the average and standard error of the mean (SEM) of six experiments where ZnO was added on the seventh pulse (■, also shown by the red bar). Mean and SEM of six controls (no addition ●). Samples from 11-20 minutes are significantly different ($P<0.05$).

Figure 6

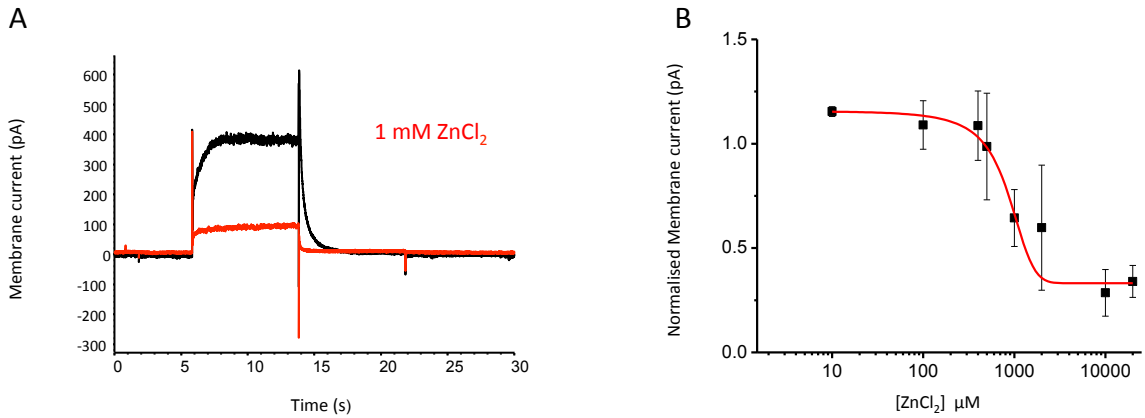

Figure 6. $ZnCl_2$ and hERG resurgent tail currents. Currents were evoked at one minute intervals from a holding potential of -70 mV, stepped to +20 mV and repolarised to -50 mV before stepping back to -70 mV. A) Addition of 1 mM $ZnCl_2$ suppressed steady state and tail currents. B) Addition of a range of $ZnCl_2$ concentrations (10 µM -10 mM) progressively suppressed the tail current. The data was well fit by a two state Boltzmann function with a half block at 890 µM (red line).

Nano-particle name	Particle origin	Nanoparticle Primary particle diameter TEM (Manufacturer)	Nanoparticle Diameter Dynamic light scattering in DW Sln 10 μg mL^{-1}	Nanoparticle Diameter Dynamic light scattering in hERG Sln. 10 μg mL^{-1}	Nanoparticle Diameter in hERG sln solution 10 μg mL^{-1}	Nanoparticle Diameter (TEM) in hERG sln solution 10 μg mL^{-1}	Zeta potential in DW/ hERG (mV)
				T=0 min	T=20 min	T=20 min	
ZnO MB	Metals Basis (Alfa Aesar)	45 +/- 30 nm	30.3 +/-6.5nm	30.3 +/-9.68 nm	37.5 +/- 7.7 nm	50.0+/- 15 nm	-5.3/-6.3
SiO_2	Sigma-Aldrich Colloidal silica HS 30	10.9 nm	10.1 +/- 0.13	10.7 +/- 1.4 nm	10.04 +/- 0.5 nm	11.7+/- 3.4 nm	-30.6/-6.3
TiO_2	Degussa Rutile	30 nm	20.0 +/-0.2 nm	40.8 +/- 2.7 nm (main peak but also significant aggregates at >50 nm)	47.1 +/-2.9 nm (main peak but also significant aggregates at >50 nm)	34.7 +/-3.4 nm	-29.8/-10. 1
MgO	Sigma-Aldrich	<50 nm	178.7 +/- 5.4 nm	92.7 +/- 10.7 nm (main peak but also significant aggregates at >100 nm)	92.7 +/- 14.7 nm (main peak but also significant aggregates at >100 nm)	ND[a]	-23.2/-4.7

Table 1 . Table showing the physical dimensions and Zeta potential (charge) of nanoparticles used in this study. Nanoparticle primary particle diameter was that provided by the manufacturers while particle size was estimated from DLS and SEM images (in the case of SiO_2, ZnO, and TiO_2 column 7) ND= not done.

Supplementary Figures

Figure S1

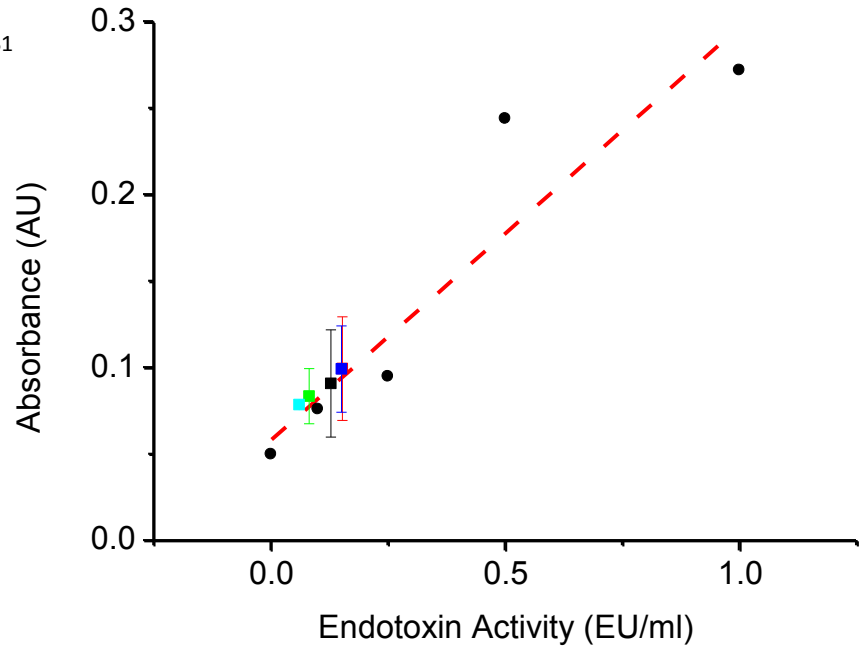

Figure S1. LAL chromogenic assay results showing standard curve (dotted red line) fit to endotoxin standards (●). The mean values of endotoxin in NPs samples at a concentrations of 10 ug/ml in hERG solution are shown. Blue, TiO_2, green, MgO_2, Black ZnO Blue SiO_2. Mean and SD of three independent measurements.

Figure S2

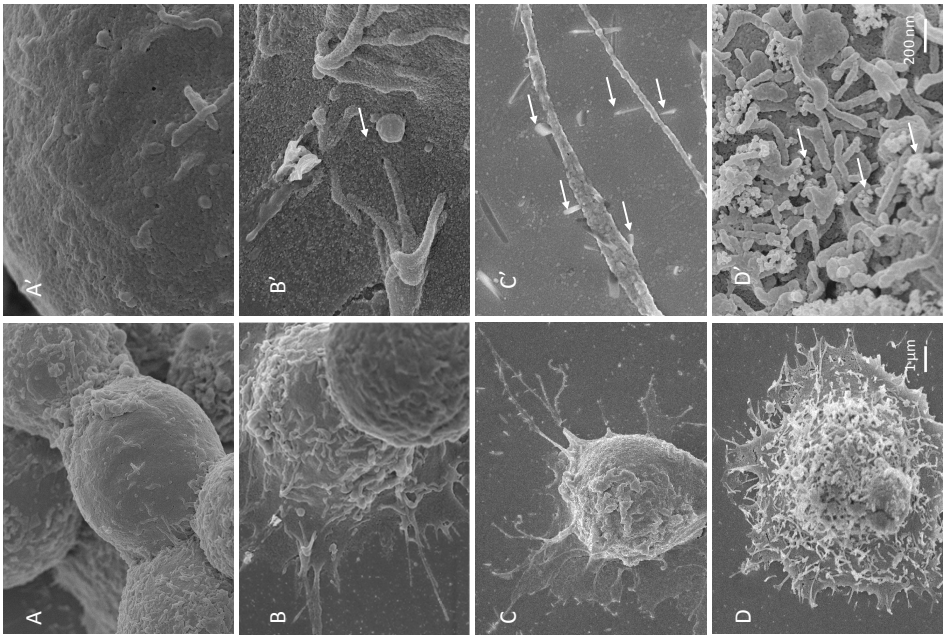

Figure S2. SEM of HEK239 cells in the presence of nanoparticles A, A' controls (no nanoparticles), B, B' SiO_2 NPs, C C' ZnO NPs (Metal Basis), D, D' TiO_2 NPs. Scale bars are 1 µM and 200 nm respectively. White arrows show a continuous covering of SiO_2 particles in B' covering the entire surface of the cell, individual ZnO crystals in C' and clusters of small spherical TiO_2 particles in D'.

Figure S3

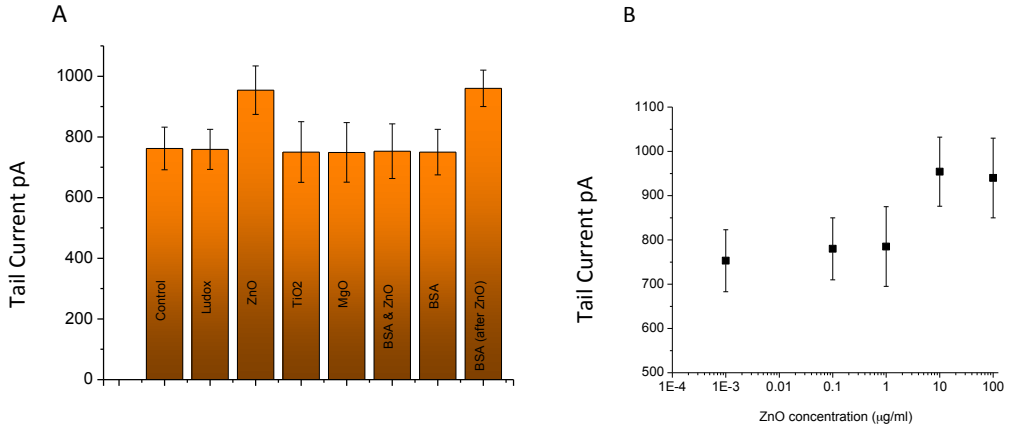

Figure S3. Summary of results from the screening of nanoparticles and the effect of coating ZnO with BSA against hERG currents. Results show the average of at least six experiments per condition. hERG currents were evoked at one minute intervals from a holding potential of -70 mV, stepped to +20 mV and repolarised to -50 mV before stepping back to -70 mV. **A,** tail current amplitudes were measured before and after addition of NPs. All NPs were added at 10 µg/ml. The ZnO sample is significantly different from the control sample ($P<0.05$). Adding BSA after induction of the ZnO effect did not reverse the increase in current. B, concentration ranges of ZnO NPs and their effects on hERG tail currents.

Figure S4

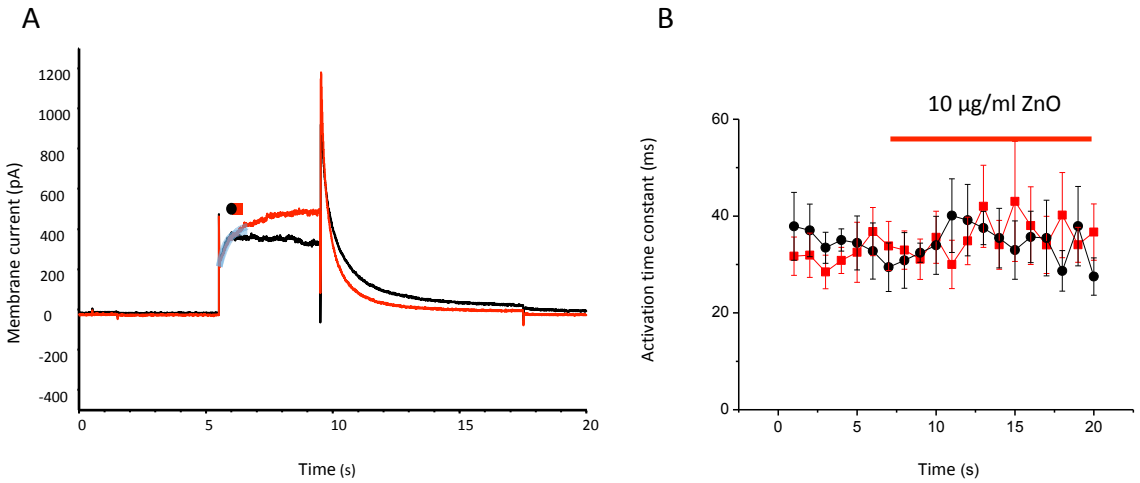

Figure S4. The effect of ZnO on activation of the hERG current. A) Examples of hERG currents evoked at one minute intervals from a holding potential of -70 mV, stepped to +20 mV and repolarised to -50 mV before stepping back to -70 mV. The example shows the first and last current after addition of ZnO. The activation was estimated by fitting the first 500 ms of the 'steady-state' currents with a single exponential function (see text). **B)** Plot of the time constant of activation of hERG in the presence and absence of ZnO over 20 minutes. Results show the average of six control (■) and six experiments where ZnO was added.

Figure S5

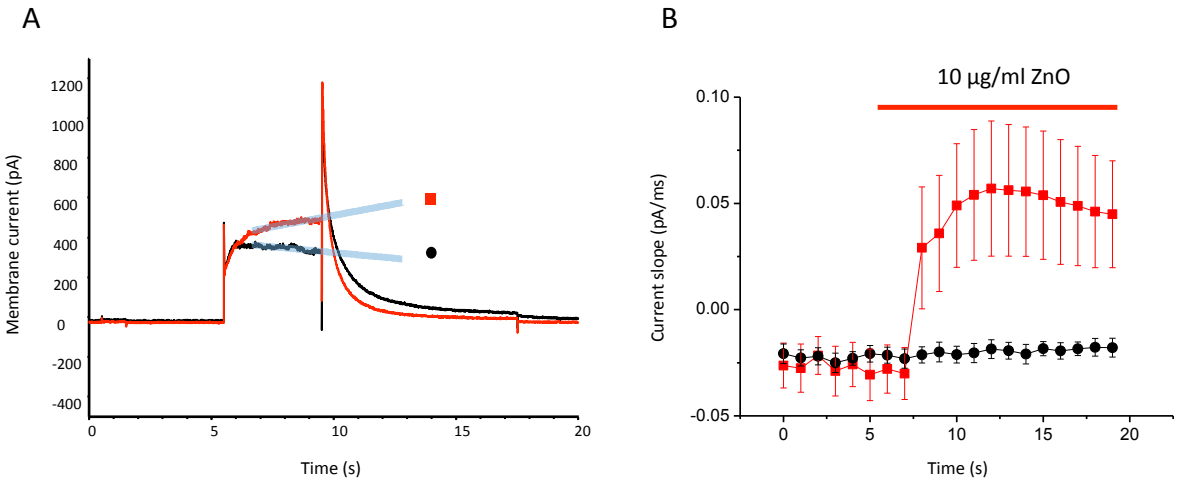

Figure S5. A) Examples of the effect of the addition of nanoparticles on the inactivation rate of the steady state hERG current. A straight line was fitted to the currents one second after initiation of the steady state current and the slope of the line plotted. **B)** Plot of the slope of the lines plotted against time. Currents are plotted against experimental time (20 minutes) as the average and standard error of the mean (SEM) of six experiments where ZnO was added on the seventh pulse (■, also shown by the red bar). The data are plotted against the mean and SEM of six controls (no addition ●).

Figure S6

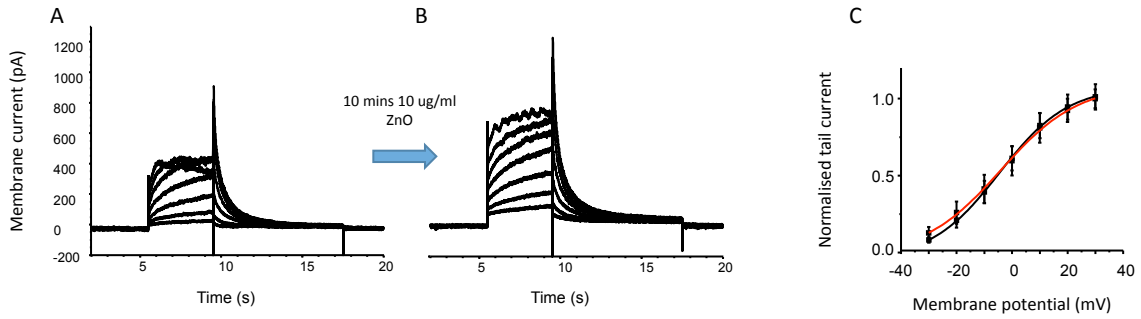

Figure S6. ZnO does not alter the current/voltage relations of the steady state or tail currents. **A)** and **B),** examples of whole-cell hERG currents before and during exposure to 10 µg/ml ZnO. There is an obvious increase in current as a result of ZnO at all voltages. **C)** Plot of tail currents *versus* voltage in ten experiments (Mean +/- SEM). The results show that both tail and steady- state currents increase proportionately at all voltages and there is no voltage shift in the peak current on ZnO addition. $V_{0.5}$ was -4.6+/- 0.42 in controls and -4.2 +/- 1.12 mV on addition of ZnO NPs, while the slope function of the Boltzmann fit was 12.36+/-0.56 and 13 +/- 1.6 mV respectively.

Figure S7

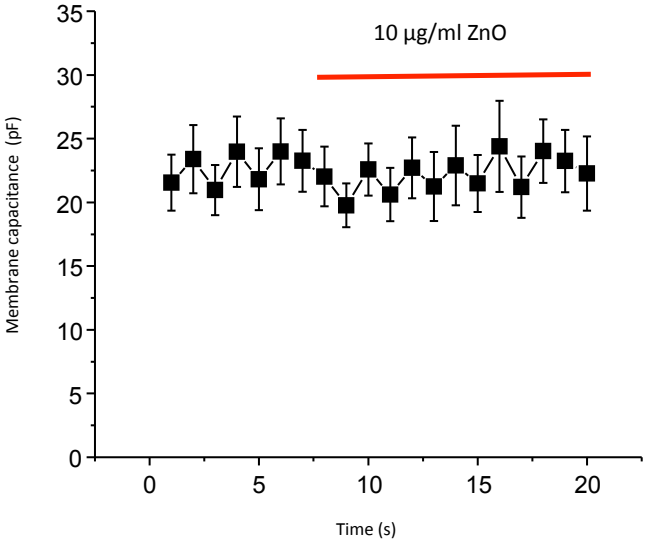

Figure S7. Membrane capacitance measured before and during ZnO NP application. The black squares represent mean and error bars +/- SEM of 6 experiments. No significant differences in membrane capacitance were detected.

Figure S8

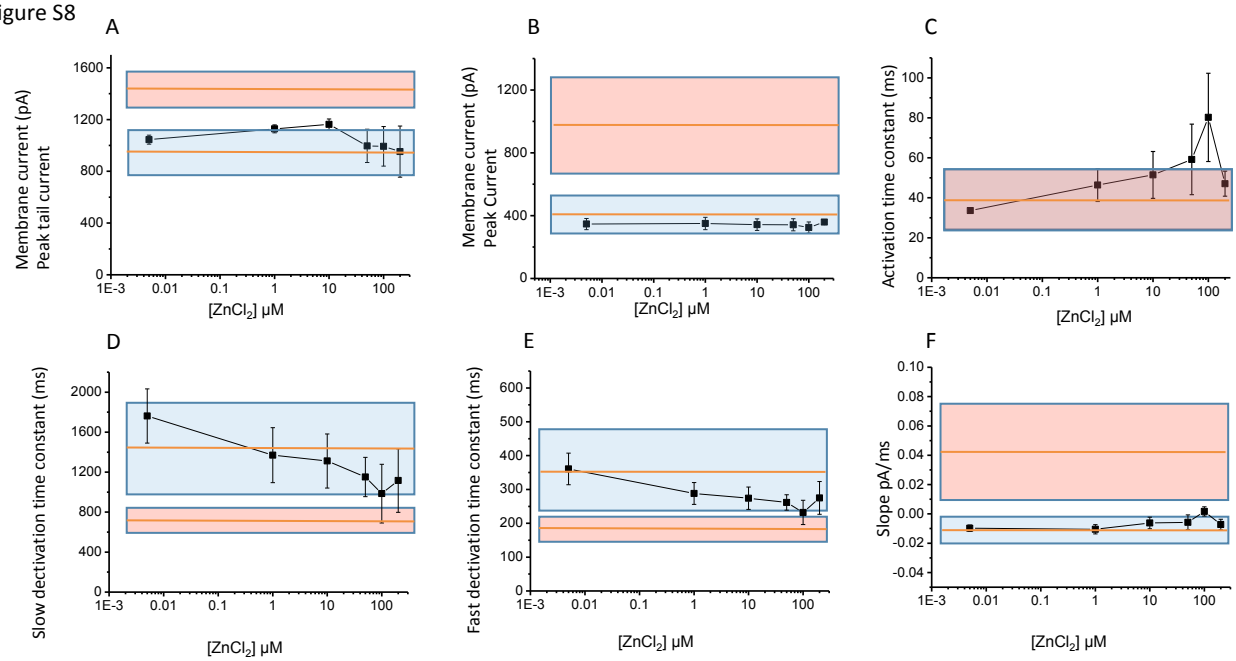

Figure S8 The effect of low concentrations of $ZnCl_2$ on hERG currents compared to the effect of 10 µl/ml ZnO. The black squares represent mean and SEM of 5 experiments in different concentrations of $ZnCl_2$ (from 1-300 µM). The blue and red boxes represent the extent of variance (SEM) and mean (red line) envelopes of control and in the presence of ZnO respectively. All currents were evoked at one minute intervals from a holding potential of -70 mV, stepped to +20 mV and repolarised to -50 mV before stepping back to -70 mV. **A)** Peak resurgent tail current**, B)** peak steady state, **C)** activation time constant of hERG current, **D)** Slow tail deactivation time constant, **E)** Fast tail deactivation time constant, **F)** slope of steady state current.

Figure S9

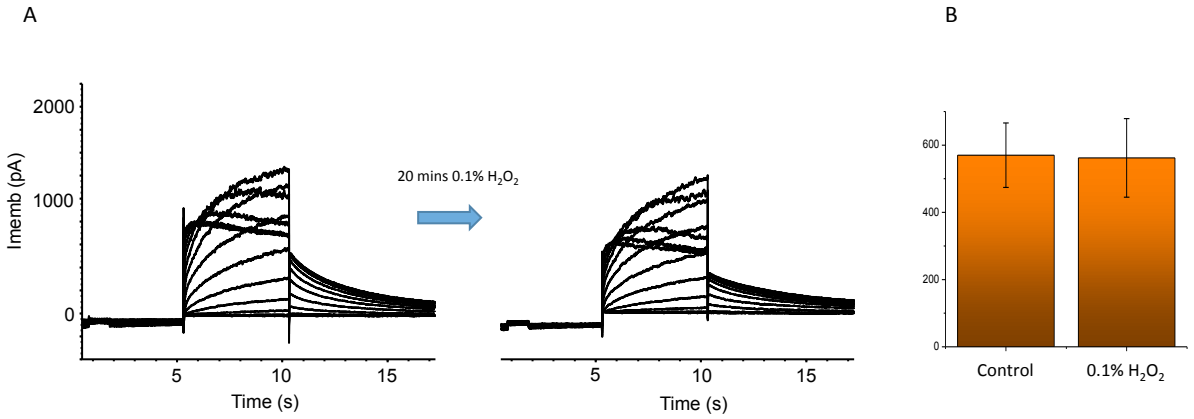

Figure S9. H_2O_2 exposure does not alter the current/voltage relations of the steady state or tail currents. **A),** examples of whole-cell hERG currents before and during exposure to 0.1% H_2O_2 (20 mins). There is a slight 'rundown' of the whole-cell current over 20 minutes and no obvious increase in current as a result of H_2O_2 exposure. **B)** Plot of the steady state currents at +20 mV in four experiments (Mean +/- SEM). The results show that steady- state currents were not altered in the short term by exposure to peroxidation.